Mechanism of Transformation of Precursors into Nanoslabs in the Early Stages of MFI and MEL Zeolite Formation from TPAOH−TEOS−H_2O and TBAOH−TEOS−H_2O Mixtures

C. E. A. Kirschhock, R. Ravishankar, L. Van Looveren, P. A. Jacobs, and J. A. Martens*

Centrum voor Oppervlaktechemie en Katalyse, K.U. Leuven, Kardinaal Mercierlaan 92, B-3001, Heverlee, Belgium

Received: January 25, 1999; In Final Form: April 12, 1999

The formation of silicate particles upon gradual addition of TEOS to concentrated TPAOH and TBAOH solutions, and upon dilution with water and aging, was studied with in situ X-ray scattering (XRS) and gel permeation chromatography (GPC). The samples for the GPC analyses were obtained by extraction of the particles from solution via a sequence of acidification with HCl, salting out with NaCl, and phase transfer into tetrahydrofuran. XRS and GPC reveal the presence of populations of particles with discrete sizes and number molecular weights, respectively, growing through aggregation. The entities forming in TPAOH are identified on the basis of their size and number molecular weight relationships with species previously identified in these suspensions by ^{29}Si NMR and other independent techniques. A mathematical expression for the X-ray scattering function is derived for particles with slab shape. When dimensions of 1.3 × 4.0 × 4.0 nm, corresponding to the nanoslab with MFI structure, or integer multiples of them are assumed, the derived function resembles the measured intensity pattern in shape and position. The observed scattering at 6.6° 2θ at very early stages is assigned to a trimer of tetracyclic undecamer. All larger particles including the nanoslab observed by XRS and GPC are multiples of this trimer. The evolution of the system in TBAOH also obeys a stacking sequence of particles of the same size, number and molecular weights, although the kinetics are totally different. Up to the formation of nanoblocks, TBAOH and TPAOH affect the reaction mixture in a very similar way, indicating that the first molecular steps in the early stages of formation of MFI and MEL zeolite structures in these systems are very similar. The nanoslabs representing a specific fragment of MFI or MEL structures have channel intersections which are at least to two sides open and contain TPA or TBA molecules, respectively. The surface of these Silicalite-1 and -2 fragments is decorated on the *ac* and *bc* planes with alkyl groups sticking out of the surface. In nanoslabs with TBA, unfavorable template−template interaction suppresses aggregation along *a* and *b*. The final product is a "double" nanoslab, probably connected along the later *c* direction of the MEL structure in which there is only a very small repulsion of the butyl chains. TPA favors particle aggregation to give larger particles measuring up to 15.6 × 8 × 8 nm, even at room temperature.

Introduction

The all-silica molecular sieve, Silicalite-1 with MFI framework topology can be crystallized by heating a mixture prepared from tetraethyl orthosilicate (TEOS), tetrapropylammonium hydroxide (TPAOH), and water.[1−3] Mixing at room temperature of TEOS and 40% concentrated TPAOH solution in TPAOH/TEOS and H_2O/TEOS with molar ratios of 0.37 and 6, respectively, leads to the selective formation of specific precursor silicate polyanions.[4,5] These were identified as the bicyclic pentamer, the pentacyclic octamer, the tetracyclic undecamer, and a trimer of the latter, counting 33 Si atoms and encasing one TPA molecule (Figure 1a−d). The largest of these silicate macromolecules (Figure 1d) has a connectivity that is already unique to the MFI zeolite framework topology.[5] Dilution with water of the concentrated solution of the trimer provokes the formation of subcolloidal particles.[3,4,6] These particles were identified as nanoslabs with very specific dimensions (Figure 1e) and with the MFI framework connectivity[4] (Figure 1e). They occlude nine TPA molecules in channel intersections and extend ca. 1.3 nm in the crystallographic *a* direction and 4.0 nm in the *b* and *c* directions of MFI framework.

Particles of such nano dimensions are too small to be observed by the traditional small angle scattering techniques (SAXS, SANS).[6,7] For the nanoslabs, an X-ray scattering (XRS) signal at about 2.8° 2θ, using CuKα radiation, was observed.[4] Smaller entities accordingly give rise to scattering at even higher angles. In this angle regime, the low angle approximation used for SAXS is no longer valid so that the trigonometric expressions cannot be linearized. This situation enticed us to have a closer look at the detected XRS phenomenon. We followed the evolution of the in situ XRS pattern in the course of transformations of precursors into nanoslabs (Figures 1d, e). Gel permeation chromatography (GPC) was handled as an independent analytic tool to analyze the molecular weight of the silicate macromolecules involved.

Silicalite-2 with MEL topology is another silica polymorph structurally related to Silicalite-1.[8−10] It crystallizes in the presence of TBAOH (tetrabutylammonium hydroxide). We used the XRS-GPC approach to gather insights into the mechanisms of Silicalite-2 versus Silicalite-1 formation.

* Corresponding author telephone, 0032-16-321637; fax, 0032-16-321998; E-mail, johan.martens@agr.kuleuven.ac.be.

10.1021/jp990298j CCC: $18.00
Published on Web 05/27/1999

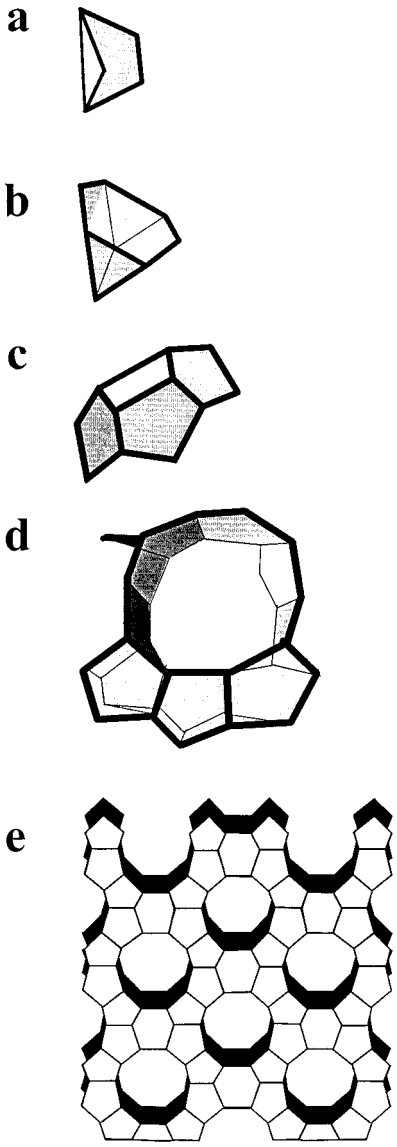

Figure 1. Siliceous entities occurring in the TPAOH−TEOS system: (a) bicyclic pentamer; (b) pentacyclic octamer; (c) tetracyclic undecamer; (d) "trimer" in mixtures with composition $(TPAOH)_{0.36}(TEOS)(H_2O)_{6.0}$; (e) nanoslab mixtures with composition $(TPAOH)_{0.36}(TEOS)(H_2O)_{17.5}$.

Experimental Section

Two Debye Scherrer diffractometers with position-sensitive detectors (5° and 40°, STOE) and CoKα1 and CuKα1 radiation were used. Data were recorded between 0.1° and 15° 2θ. At regular intervals, the intensity of the incident beam and the retainment of diffractometer settings were checked by measurement of a standard (Si) and a water-containing capillary. Between measurements the beam catch was not moved. The samples were adjusted by eyesight. The diffractograms were corrected by subtraction of the background measured with the water sample.

Mixtures were prepared by addition of 10 mL of TEOS (Acros, 98%) in steps of 1 to 9 mL of the template TPAOH (Fluka, 40%) or TBAOH (Aldrich, 40%). After each addition, the mixture was stirred for a few minutes. For the XRS measurements, a small amount of liquid was filled in a capillary with 1 mm diameter and sealed. The diffractograms of the liquids in the capillaries did not change with time, even after 5 days. Mixtures of TPAOH and TEOS displayed phase separation

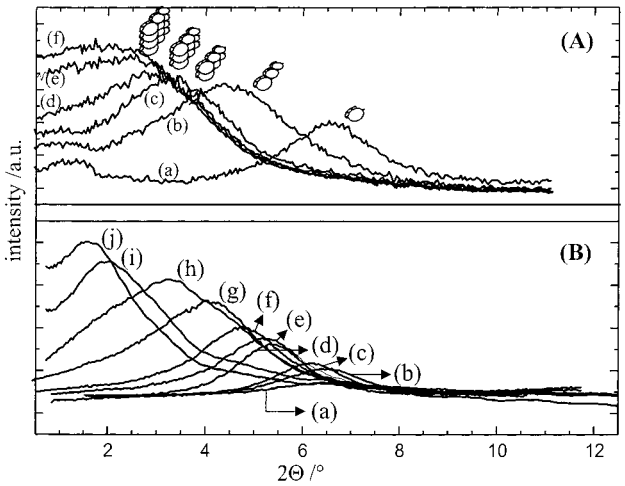

Figure 2. XRS by small species present in the mixtures of TEOS with (A) TPAOH: (a) 4 mL, (b) 7 mL, (c) 10 mL TEOS added; (d) directly after addition of water, (e) 2 h later, and (f) 12 h after water addition and (B) (a−c) 1, 2, and 3 mL of TBAOH added, (d−f) 5, 6, and 7 mL added, (g, h) 8 and 10 mL added, (i) directly after water addition, and (j) 10 h later.

until the fourth TEOS addition. At this point stirring of the liquid during 40 min prior to sampling was required to obtain an XRS pattern that changed no more with time. With TBAOH, there was no phase separation observed.

After addition of all TEOS, 9 mL of water was added. A sample was taken and its evolution followed in situ for 24 h. Comparison with diffractograms of the remaining batch gave a similar diffraction pattern, thus precluding influences of the capillary.

The number average molecular weight (M_n) of the silicon particles was determined on a high pressure liquid chromatograph (Hewlett-Packard 1090) with a RI detector (Hewlett-Packard 1047A) and Chrompack Microgel 3 mix column (length 25 cm, i.d. 7.7 mm). A guard column with the same polymeric packing was used in conjunction. The samples were diluted in THF (10 wt % sample material) and passed through a filter ($<0.5\ \mu$m) prior to injection (20 μL). The flow rate of the mobile phase was 1 mL min^{-1} at an overall pressure not exceeding 6 MPa. The column/detector temperature was 40 °C. The molecular weight distribution was referred to polystyrene standards (Chrompack, Polymer Laboratories Ltd.).

The TPA-silicate THF solution was prepared following the earlier reported procedure[4a] and concentrated before the extraction procedure. The homogeneous concentrated solution was used for GPC analysis.

Results and Discussion

TEOS−TPAOH−Water System. A representative sequence of XRS patterns of the TPAOH system is shown in Figure 2A. The scattering angles decrease with addition of the aliquots of TEOS and later upon water addition and aging, indicating growth of the scattering entities. Similar X-ray scattering in the low angle regime by uniform, small entities was previously observed in TPA-silicate gel.[11] Lacking information on the geometry of the scattering entities, those data were discussed in terms of characteristic lengths present in the sample.

Assuming that particles with slab shape are dealt with,[4] in the supplementary information a mathematical expression for the scattering function is derived for uniform, isolated particles lacking an inner structure. The shape of the scattering function mirrors the distribution of possible trajectories through the slab.

TABLE 1: XRS Signal Intensity upon Addition of TEOS to TPAOH with the Evolution of Species

$vol_{(TEOS)}$ (mL)	nb int[a] (%)	d_{exptl} (nm)	d_{calc} (nm)	c (nm)	b (nm)	a (nm)	in int[b] (%)	d_{exptl} (nm)	d_{calc} (nm)	b (nm)	c (nm)	a (nm)
4	29	1.35	1.353	1.33	1.0	1.3	1.0	6.69	5.784	4.0	8.0	1.3
7	74	1.99	2.004	2.67	1.0	1.3	4.0	7.006				
10	96	2.60	2.767	4.00	1.0	1.3	4.0	6.986				
time (h)												
0.66	90	3.160	2.981	4.00	2.0	1.3	12	7.269	7.288	8.0	8.0	1.3
1.3	82	3.306	3.306	4.00	3.0	1.3	20	8.071	7.969	8.0	8.0	5.2
1.99	77	3.357	3.715	4.00	4.0	1.3	27	9.580	9.812	8.0	12.0	5.2
3.31	72	3.572					30	10.756	10.494	8.0	12.0	7.8
4.70	70	3.546					31	11.517	11.953	12.0	12.0	7.8
8.70	70	3.660	3.715	4.00	4.0	1.3	31	11.389				
18.00	70	3.833					31	11.389				
23.00	70	3.833					32	11.389				
24.00	68	3.768					32	11.648				

[a] nb int: Normalized intensity of nanoblocks. [b] in int: Normalized intensity of intermediates.

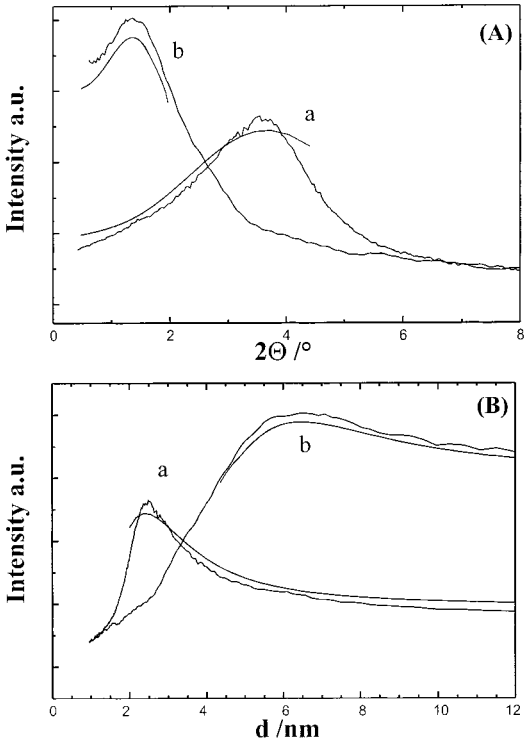

Figure 3. Comparison of calculated scattering with two representative measured data sets: (A) 2θ scaling and (B) d scaling (a) system after addition of 8 mL template and (b) after dilution with water and 10 h aging. The simulated patterns are depicted only in the region where the mathematical derivation of the structure factor is valid.

In the expression against 2θ, the intensity function resembles a Lorentzian so that this profile was selected for the fitting of the XRS data. When dimensions of $1.3 \times 4.0 \times 4.0$ nm (nanoslab, Figure 1e) or integral multiples of them are assumed, the derived function resembles the measured intensity pattern in shape and position. Some examples of fittings are shown in Figure 3. According to the scattering function, the d value at maximum XRS intensity is related to the diagonal in space, D, of the slab

$$d = 0.64D \tag{1}$$

The low angle region of all diffractograms could be fitted by one or two Lorentzian lines corresponding to one or two populations of differently sized particles. Measured d values and calculated d values, assuming specific dimensions related to the nanoslab, are summarized in Table 1.

The 33 Si atom containing precursor molecule previously identified with ^{29}Si NMR roughly has dimensions of $1.3 \times 1.3 \times 1$ nm (Figure 4). The corresponding diagonal in space, D, is 2.1 nm. It corresponds to a d value of 1.3 nm, or a 2θ value of 6.6°. This is exactly the position of the scattering signal in the sample after addition of 4 mL of TEOS after 40 min stirring time (Figure 2A, Table 1). One of the final observed d values of ca. 3.8 nm (Table 1) corresponds to a slab with a diameter in space, D, of 5.8 nm, matching with the nanoslab. The assignment of the other observed d values was possible with the information from GPC analysis.

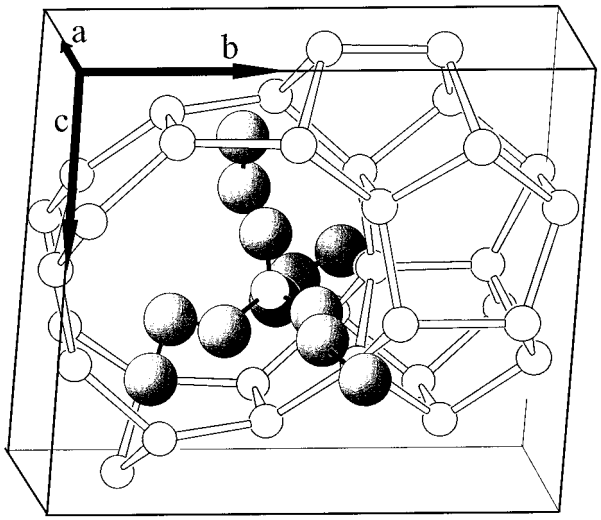

Figure 4. Precursor containing a TPA cation. The precursor's dimensions and crystallographic directions are indicated.

The relative number molecular weights of the silicate macromolecules, extracted from the solutions using a procedure involving acidification, salting out, and phase transfer into organic solvent,[4] were determined with GPC. Two samples were prepared by extracting the silica particles after 10 and 45 min of mixing of TEOS with concentrated TPAOH, respectively. The chromatograms displayed several peaks with a molecular weight relationship corresponding to monomer, dimer, trimer, hexamer, and nonamer (Figures 5, 6). Two further samples prepared by addition of water and stirring for 10 and 45 min, respectively, revealed larger structures characterized by smaller elution volumes. These entities have number molecular weights corresponding to 18-mer, 27-mer, 36-mer, and some heavier species up to the 108-mer.

An attempt was made to assign masses based on the calibration curves for polystyrenes. For this exercise, possible monomers were assumed to be the bicyclic pentamer (Figure 1a) or the tricyclic undecamer (Figure 1c), abundantly present

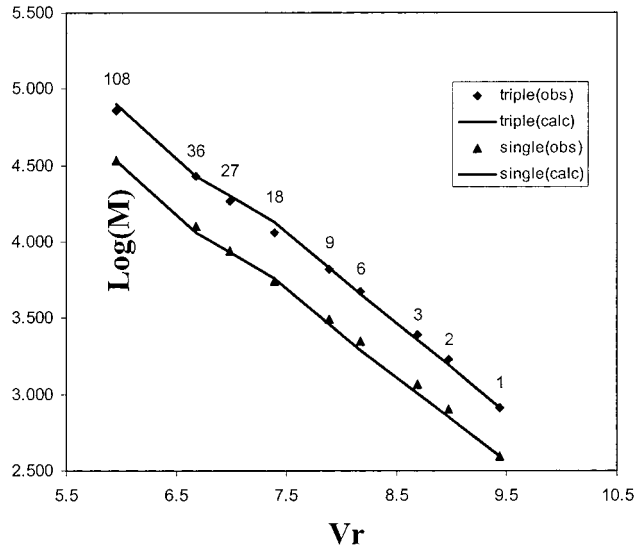

Figure 5. Logarithmic molar masses versus the observed and calculated retention volumes for two of the assumed precursors. Single refers to the bicyclic pentamer (Figure 1a), triple to the tetracyclic undecamer (Figure 1c) assumed as precursor.

at early times in these liquids.[5] It turned out that these two monomers and their respective oligomers fitted equally well with the observed retention volumes (Figure 6). A similar agreement was obtained for the pentacyclic octamer (Figure 1b). The assumption of larger entities as monomer resulted in less convincing fits of the GPC data.

The dimer was observed to give a split chromatographic peak (indicated as 2 and 2′ in Figure 6) which helped the final assignment. Among the three suggested monomers, only the tricyclic undecamer can be connected according to two different modes, resulting in two geometrically different dimers, both being a fragment of MFI framework. Addition of a third monomer to either of these dimers results in the formation of the trimer (Figure 1d).

Assuming the tricyclic undecamer as the monomer, all heavier particles observed by GPC are multiples of the trimer of it (Figures 6 and 7). Shortly after the dilution with water, larger entities are detected which are formed by aggregation, resulting in structures containing 18, 27, and 36 monomers, or 6, 9, and 12 trimers, respectively. The largest of these particles corresponds to the nanoslab (Figure 1e). The nanoslab is indeed selectively formed under such conditions,[4] supporting the assignment of the monomer.

Following this interpretation of the GPC peaks (Figure 6), the diagonals in space determined by XRS should correspond to those of particles built from integral multiples of the trimer, representing a volume of ca. 1.3 × 1.0 × 1.3 nm (Figure 4). Indeed, all XRS signals can be explained following this assumption (Table 1). After addition of 4 mL of TEOS and stirring for 40 min, the trimer is selectively formed. Further addition of TEOS to total amounts of 7 and 10 mL gives rise to particles having a doubling and tripling of the 1.3 nm dimension, respectively. The most likely direction for this coupling of precursors is via the small sides in the later *c* direction of the MFI structure (Figure 4). When trimer molecules are approaching each other along this direction, there is a minimum sterical repulsion by propyl groups of occluded TPA (Figure 4). According to the XRS data, the linking of trimers along *c* is terminated after three units (Table 1). Growth along *c* is a major issue in the mechanism of formation of MFI zeolites and will also be encountered later.[15] Several groups reported the growth along *c* to be the fastest.[16−19]

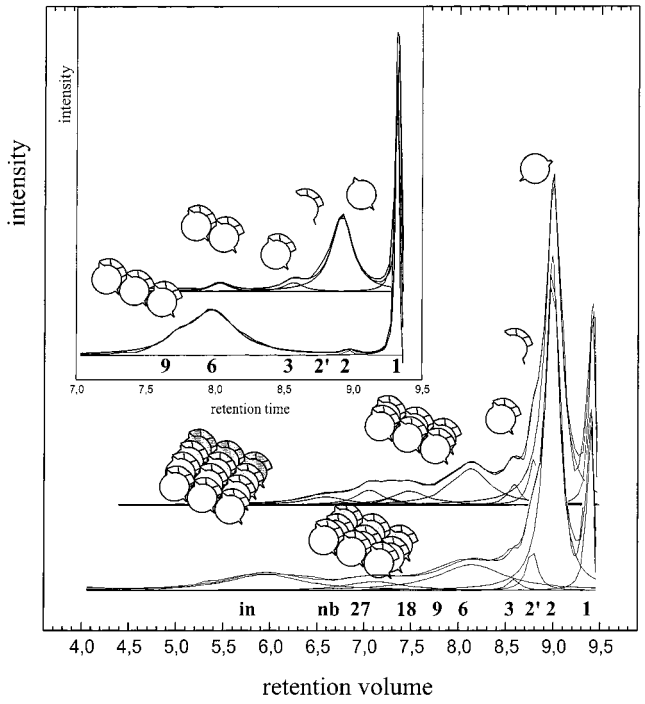

Figure 6. Measured and fitted GP chromatograms. Data before water addition are shown in the inset (top, after 10 min; bottom, after 45 min mixing time). After the addition of water (upper chromatogram, 10 min after water addition; lower chromatogram, after 45 min) immediately larger aggregates are observed.

In the first 2 h after addition of water, the nonamers are coupled in the later *b* direction of the MFI structure (Table 1, Figure 7). The termination of the linking along *c* and the switching to coupling along the *b* direction may be the result of a lack of static stability of long chains (Figure 7). So before further aggregation along *c* can proceed, the entities preferentially grow first in the *b* direction. Four nonamers stacked along *b* inevitably conclude in the formation of the nanoslab (Table 1, Figure 7). These nanoslabs are present throughout the crystallization of Silicalite-1 upon heating of such solutions[1−4,12] and, therefore, are quite stable entities.

The trimer was observed by GPC among the species that were extracted after only 10 min reaction time (Figure 6), whereas in the in situ NMR[5] and XRS studies (Figure 2A), this entity was not observed before at least 30 min have passed. After 45 min of reaction, the extracts examined with GPC even contained aggregates of the trimer (Figure 6), which by in situ XRS are observed only after the addition of water (Figure 2A). This is not necessarily a contradiction because the extraction procedure, involving acidification and addition of sodium chloride, can be expected to speed up the aggregation.[13]

In the aging period after water addition, larger structures designated as "intermediates" are formed by coupling of nanoslabs. These structures correspond to two to three stackings of nanoslabs in the *b* and *c* directions and up to a stack of six of them in the *a* direction (Table 1). Upon addition of water, the nanoslab (1.3 × 4 × 4 nm) is immediately stacked into blocks of 1.3 × 8 × 8 nm, 5.2 × 8 × 8 nm, and, finally, into structures counting 48 nanoslabs, corresponding to twelve 1.3 × 8 × 8 nm sheets, stacked along *a*.

The mechanism of particle growth as presented above corresponds to a cluster−cluster growth mechanism,[14] which is well-known in sol−gel chemistry. It was also suggested as a likely pathway for the formation of nanoscopic particles in mixtures containing TEOS, TPAOH, and water.[7,13]

TABLE 2: XRS Signal Intensity upon Addition of TEOS to TBAOH with the Evolution of Species

$vol_{(TEOS)}$ (mL)	nb int[a] (%)	d_{exptl} (nm)	d_{calc} (nm)	*c* (nm)	*b* (nm)	*a* (nm)	$vol_{(TEOS)}$ (mL)	nb int[a] (%)	d_{exptl} (nm)	d_{calc} (nm)	*c* (nm)	*b* (nm)	*a* (nm)
1	10	1.383	1.353	1.33	1.0	1.3	6	63	1.864				
2	21	1.383					7	69	2.110	2.004	2.67	1.0	1.3
3	30	1.428					8	80	2.680	2.767	4.0	1.0	1.3
4	40	1.640					10	100	2.978	2.981	4.0	2.0	1.3
5	51	1.700											

time (h)	nb int[a] (%)	d_{exptl} (nm)	d_{calc} (nm)	*c* (nm)	*b* (nm)	*a* (nm)	in int[b] (%)	d_{exptl} (nm)	d_{calc} (nm)	*b* (nm)	*c* (nm)	*a* (nm)
0.25	27	3.235	3.306	4.0	3.0	1.3	86	5.413				
1.25	11	3.266					92	5.550				
3.76	10	3.347					93	5.649				
6.76	9	3.495					92	5.767	5.784	4.0	8.0	1.3
10.0	8	3.527	3.715	4.0	4.0	1.3	92	5.883				
15.00	8	3.527					92	5.883				
20.00	8	3.527					92	5.883				
24.00	8	3.527					92	5.883				

[a] nb int: Normalized intensity of nanoblocks. [b] in int: Normalized in tensity of intermediates.

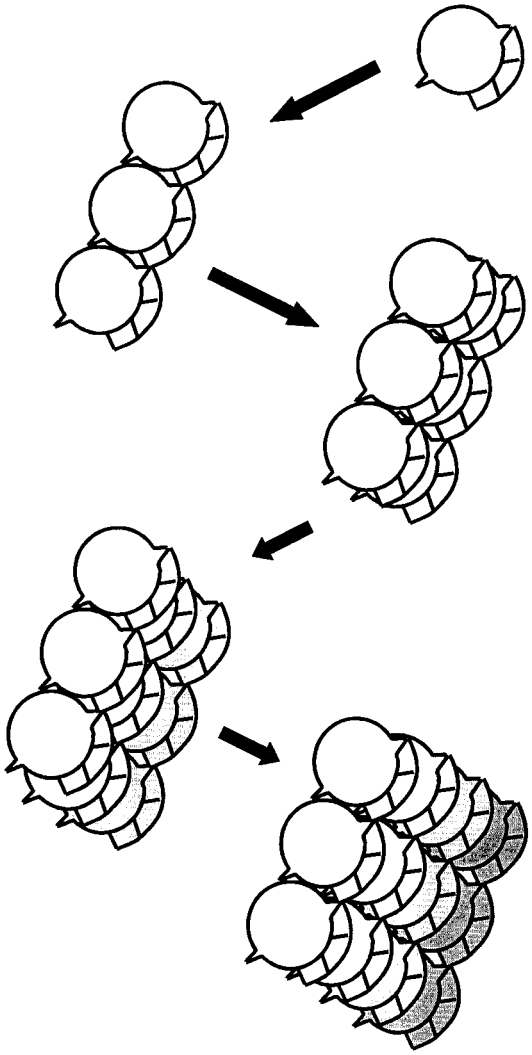

Figure 7. Schematic presentation of nanoslab formation as determined by XRS and GPC.

TEOS−TBAOH−Water System. In a similar series of XRS experiments, TPAOH was replaced by TBAOH (Figure 2B). During the TEOS addition steps, the XRS signals closely resembled the TPAOH system (Figure 2A). A scattering which can be assigned to a particle of the same size as the trimer is already observed after the first addition of TEOS to TBAOH. Measured *d* values and the most closely matching calculated *d* values, assuming particles composed of 1.3 × 1.0 × 1.3 nm scattering volumes, are summarized in Table 2. The evolution of the system also obeys a stacking sequence as observed in the TPAOH system, although the nanoslab (1.3 × 4.0 × 4.0 nm) is detected at a later time (10 h) after water addition (Table 2).

In the GPC analysis of extracts, the retention volumes were similar to those obtained with TPAOH. The chromatographic peaks of hexamer and nonamer were relatively less intense, however. Thus it can be deduced that the formation of a trimer leading to the MEL structure follows the same path as that of the trimer for MFI, although the subsequent aggregation to form nanoslabs is more hindered. The final scattering at 1.5° (CuKα) (Figure 2B) can be accounted for by slabs with dimension of 8.0 × 4.0 × 1.3 nm (Table 2). Unfortunately, the particle extraction procedure failed with samples to which the water was added. Instantaneous gelling occurred upon acidification.

Up to the formation of nanoblocks, TBAOH and TPAOH affect the reaction mixture in a very similar way. Every channel intersection in a nanoslab prepared with TPAOH is occupied by a TPA.[4] Intersections of nanoslabs prepared with TBAOH are most likely filled by TBA. This position of template molecules has been calculated to be an energetically most favorable arrangement for TPA in MFI, but causes repulsive intermolecular forces for TBA in bulk MFI and MEL.[10,20,21] The observation of the nanoslab with TPA as well as with TBA indicates that, in this structural unit, the template−template interaction is different than in bulk material. This can directly be related to the geometry of the structural units. Whereas the straight channels of bulk MFI and one of the straight channels of MEL already are formed, only fragments of the sinusoidal channels in MFI or the second set of straight channels in MEL are present. Thus, all of the cavities in the extended structure are at least to two sides open, allowing for an evasion of unfavorable intermolecular interaction of TBA. Hence, the surface of these Silicalite-1 and -2 fragments is decorated on the *ac* and *bc* planes with alkyl groups sticking out of the surface. This explains the observation of dimers in the case of TBA. Here the template−template interaction suppresses aggregation along *a* and *b*. These "double" nanoslabs are most probably connected along the later *c* direction of the MEL structure. In this direction only a very small repulsive contribution of the butyl chains of occluded TBA is expected.[15] TPA on the other hand favors particle aggregation to give MFI.[10,20,21] Thus, even during hydrolysis before raising the temperature to 100 °C larger entities (intermediates) stacked along *a* can be

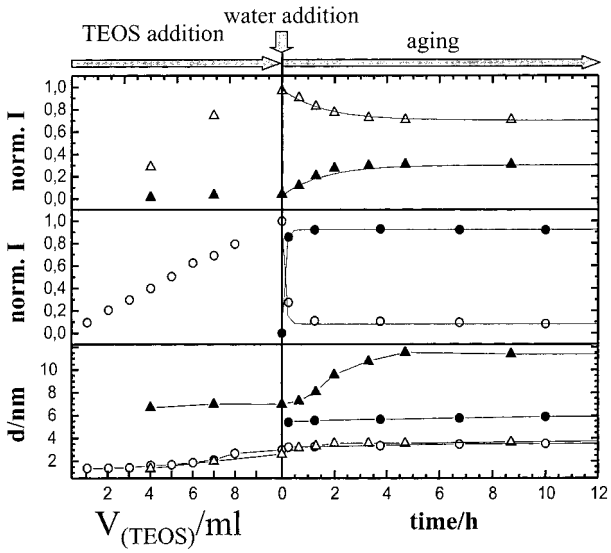

Figure 8. Quantitative evolution of the normalized XRS intensities (norm. I). The continuous lines in the upper two diagrams are calculated using the determined rate constants (Table 3). The lower part compares the evolution of the measured *d* values in the TPAOH (triangles) and TBAOH (circles) systems. The open symbols (△ and ○) represent the particles in the range from trimer to nanoslabs and the closed symbols (▲ and ●) represent the particles with sizes larger than the nanoslabs (intermediates).

obtained. In these particles, the inner cavities are already completed cross-sections of sinusoidal and straight channels surrounded by four template molecules in neighboring crossings.

Quantification

According to the derived scattering function, the scattering intensity is proportional to the volume of the particles and reaches a maximum for cubelike entities. The measured intensity is not only dependent on the scattering volume and particle geometry but is also a rather complex function of angle and experimental setup. In a first approach, the area under the signals was used as a measure of the total volume of the respective particles. It was assumed that all silicon is present in the scattering entities. This assumption is based on the former observation that almost all silicon in these mixtures is incorporated into these structures, first in the precursor species,[5] and later in the nanoslabs.[4]

With these normalization factors, a linear dependency of scattered intensity on the amount of TEOS added to the TPAOH and TBAOH was observed (Tables 1 and 2, Figure 8). It means that TEOS is quickly converted into scattering entities and supports the normalization procedure.

In the TPAOH system and after addition of water, the volume of nanoslabs and smaller particles decreases in favor of intermediates until ca. 30% of the nanoslabs are converted into intermediates (Figure 8, Table 1). The ca. 70% nanoslabs corresponds nicely to the extraction yield of such particles from these solutions[4] and supports the validity of the normalization factors. The present data (Figure 8) show that the 30% of the silicon not susceptible to extraction is present as larger MFI-type particles.

The evolution of the volume of nanoslabs and intermediates with time can be described by reaction kinetics approaching equilibrium (Figure 8):

$$\text{nanoslabs} \underset{k^{-1}}{\overset{k^{1}}{\rightleftharpoons}} \text{intermediates} \qquad (2)$$

TABLE 3: Apparent Rate Constants for the Transformation of Nanoblocks to Intermediates upon Using Different Alkylammonium Hydroxides

	TPAOH	TBAOH
k^1 [h^{-1}]	0.19	9.79
k^{-1} [h^{-1}]	0.44	0.85

Regarding the complex stepwise aggregation observed with TPAOH (Table 1), this is of course a simplification because of the lumping of nanoslabs with all smaller entities and of the different kinds of intermediates. The apparent first-order rate constants derived from the data are given in Table 3. The TEOS polycondensation in TBAOH is already finished after half an hour and the equilibrium (eq 2) is shifted far to the right. Almost 90% of the nanoslabs are converted into intermediates composed of two nanoslabs. As only one step is necessary to reach the product, the reaction is faster than with TPAOH, for which the final intermediate is the product of multiple aggregations involving also difficult linkages along the large faces of the slabs. With TPAOH, the equilibrium is only reached after 6 h and only 30% of the nanoslabs is converted into intermediates. The observation of equilibria between strictly limited sizes of the thin sheets reflects mechanic stability effects of these subcolloidal entities in a liquid medium and the tendency for aggregation of the blocks along *a*, *b*, and *c*. A more detailed discussion of the aggregation of the nanoslabs in terms of the potential energy barriers will be presented elsewhere.[15] There also the formation of crystalline colloidal MFI-type material from the presently characterized mixtures which will be described. It will be shown that heating of the clear solution shifts the equilibria of nanoblocks and intermediates toward the aggregates which then form the final product of the clear solution synthesis.

Acknowledgment. This work was sponsored by the Belgian Government in the frame of IUAP-PAI (postdoctoral fellowship to C.E.A.K.) and by the Flemish Fund for Scientific Research. R.R. acknowledges K.U. Leuven for a postdoctoral fellowship and L.v.L., the Flemish IWT for a fellowship.

Supporting Information Available: Mathematical expression for the scattering function. This material is available free of charge via the Internet at http://pubs.acs.org.

References and Notes

(1) Schoeman, B. J. *Zeolites* **1997**, *18*, 97.
(2) Schoeman, B. J. *Microporous Mater.* **1997**, *9*, 267.
(3) Schoeman, B. J.; Regev, O. *Zeolites* **1996**, *17*, 447.
(4) (a) Ravishankar, R.; Kirschhock, C.; Schoeman, B. J.; Vos, D. D.; Grobet, P. J.; Jacobs, P. A.; Martens, J. A. *Proceedings of the 12th International Zeolite Conference*; Treacy, Marcus, Bisher, Higgins, Eds.; Materials Research Society: Pennsylvania, 1999; Vol. III, p 1825. (b) Ravishankar, R.; Kirschhock, C. E. A.; Knops-Gerrits, P. P.; Feijen, E. J. P.; Grobet, P. J.; Vanoppen, P.; De Schryver, F. C.; Miehe, G.; Schoeman, B. J.; Jacobs, P. A.; Martens, J. A. *J. Phys. Chem. B* **1999**, *103*, 4960.
(5) Kirschhock, C. E. A.; Ravishankar, R.; Verspeurt, F.; Grobet, P. J.; Jacobs, P. A.; Martens, J. A. *J. Phys. Chem. B* **1999**, *103*, 4965.
(6) de Moor, P.-P. E. A.; Beelen, T. P. M.; van Santen, R. A. *Microporous Mater.* **1997**, *9*, 117.
(7) Beelen, T. P. M.; Dokter, W. H.; van Garderen, H. F.; van Santen, R. A. In *Synthesis of Porous Materials, Zeolites, Clays, and Nanostructures*; Occelli, Kessler, Eds.; Dekker Inc.: New York, 1997; p 59.
(8) Fyfe, C. A.; Gies, H.; Kokotailo, G. T.; Pasztor, C.; Strobl, H.; Cox, D. E. *J. Am. Chem. Soc.* **1989**, *111*, 235.
(9) Koningsveld, H. V.; Jansen, J. C.; van Bekkum, H. *Zeolites* **1990**, *10*, 235.
(10) Buchart, E. D. V.; Koningsveld, H. V.; Graaf, B. V. D. *Microporous Mater.* **1997**, *8*, 215.
(11) Perego, G.; Millini, R.; Perego, C.; Carati, A.; Pazzuconi, G.; Bellussi, G. *Stud. Surf. Sci. Catal.* **1997**, *105*, 205.
(12) Watson, J. N.; Iton, L. E.; Keir, R. I.; Thomas, J. C.; Dowling, T. L.; White, J. W. *J. Phys. Chem. B* **1997**, *101*, 10094.

(13) Schoeman, B. J. *Microporous Mesoporous Mater.* **1998**, *22*, 9.

(14) Brinker, C. J.; Scherrer, G. W. In *Sol−Gel Science, The Physics and Chemistry of Sol−Gel Processing*; Harcourt Brace Jovanovich: Boston, 1990.

(15) Kirschhock, C. E. A.; Ravishankar, R.; Jacobs, P. A.; Martens, J. A., manuscript under preparation.

(16) Jansen, J. C.; Engelen, C. W. R.; van Bekkum, H. In *Zeolite Synthesis*; Ocelli and Robson, Eds.; ACS Symposium Series 398; American Chemical Society: Washington, DC, 1989; p 257.

(17) Iwasaki, A.; Hirata, M.; Kudo, I.; Sano, T.; Sugawara, S.; Ito, M.; Watanabe, M. *Zeolites* **1995**, *15*, 308.

(18) Iwasaki, A.; Hirata, M.; Kudo, I.; Sano, T. *Zeolites* **1996**, *16*, 35.

(19) Cundy, S. C.; Lowe, B. M.; Sinclair, D. M. *Faraday Discuss.* **1993**, *95*, 235.

(20) Shen, V.; Bell, A. T. *Microporous Mater.* **1996**, *7*, 187.

(21) Lewis, D. W.; Freeman, C. W.; Catlow, C. R. A. *J. Phys. Chem.* **1995**, *99*, 11194.